

PAPER

Antibacterial activity and biocompatibility of zein scaffolds containing silver-doped bioactive glass

To cite this article: Aiah A El-Rashidy *et al* 2018 *Biomed. Mater.* **13** 065006

View the [article online](#) for updates and enhancements.



IOP | ebooks™

Bringing you innovative digital publishing with leading voices to create your essential collection of books in STEM research.

Start exploring the collection - download the first chapter of every title for free.

Biomedical Materials



PAPER

Antibacterial activity and biocompatibility of zein scaffolds containing silver-doped bioactive glass

RECEIVED
9 April 2018

REVISED
4 August 2018

ACCEPTED FOR PUBLICATION
8 August 2018

PUBLISHED
24 August 2018

Aiah A El-Rashidy^{1,8} , Gihan Waly¹, Ahmed Gad^{2,3}, Judith A Roether⁴, Jasmin Hum⁵, Yuyun Yang^{5,6}, Rainer Detsch⁵, Azza A Hashem¹, Inas Sami¹, Wolfgang H Goldmann⁷ and Aldo R Boccaccini^{5,8} 

¹ Department of Biomaterials, Faculty of Dentistry, Cairo University, 11562 Cairo, Egypt

² Department of Animal Production, Faculty of Agriculture, Cairo University, 12613 Giza, Egypt

³ Cairo University Research Park (CURP), Faculty of Agriculture, Cairo University, 12613 Giza, Egypt

⁴ Institute of Polymer Materials, University of Erlangen-Nuremberg, D-91058 Erlangen, Germany

⁵ Institute of Biomaterials, University of Erlangen-Nuremberg, D-91058 Erlangen, Germany

⁶ Institute of Surface/Interface Science and Technology, Department of Material Science and Chemical Engineering, Harbin Engineering University, Harbin, China

⁷ Biophysics Group, Department of Physics, University of Erlangen-Nuremberg, D-91052 Erlangen, Germany

⁸ Authors to whom any correspondence should be addressed.

E-mail: aiah.abdelwahab@dentistry.cu.edu.eg and aldo.boccaccini@ww.uni-erlangen.de

Keywords: zein scaffolds, bioactive glass, silver, *in vitro* biocompatibility, antibacterial

Supplementary material for this article is available [online](#)

Abstract

Composite 3D scaffolds combining natural polymers and bioceramics are promising candidates for bone tissue engineering (BTE). Zein, as a natural plant protein, offers several advantages, including biocompatibility, adequate strength properties, and low/no immunogenicity; however, it lacks bioactivity. Thus, composite zein: bioactive glass (BG) scaffolds are proposed as promising candidate for BTE applications, with silver-doping of bioactive glass providing an antibacterial effect against possible post-implantation infection. Therefore, the aim of this study was to investigate the *in vitro* antibacterial properties, biocompatibility, bioactivity and compressive strength of zein scaffolds containing silver-doped bioactive glass. BG nanoparticles, undoped and Ag-doped, were fabricated using the sol-gel method. 3D composite zein:BG scaffolds, containing 20 wt% BG, were prepared and their antibacterial activity against *Escherichia coli* (*E. coli*) and *Staphylococcus aureus* (*S. aureus*) was assessed using the disc diffusion assay. Human osteoblast-like MG-63 cells were used to evaluate the *in vitro* biocompatibility of the prepared scaffold groups. In addition, the compressive strength of the scaffolds was determined using uniaxial compression strength testing and the scaffold interconnected porosity was measured using helium pycnometer. Disc diffusion assay showed that only zein scaffolds containing Ag-doped sol-gel BG are antibacterially positive against *E. coli* and *S. aureus*. Pure zein scaffolds and zein scaffolds containing sol-gel-derived BG showed no negative influence on the growth of MG-63 cells, as evident by the cells' ability to survive, proliferate, and function on these scaffolds. Moreover, incorporating sol-gel-derived BG into zein scaffolds at zein:BG of 80:20 ratio showed bioactive properties with adequate porosity without affecting the scaffolds' compressive strengths, which was similar to that of trabecular bone, suggesting that the new composites have potential for BTE applications in non-loaded bearing areas.

1. Introduction

Tissue engineering (TE) is an effective treatment modality for regeneration of bone defects larger than critical defect size. The simplest paradigm of TE utilizes a scaffold as temporary extracellular matrix to

support cell attachment and proliferation. For the TE scaffold to perform this critical function, it should fulfill certain requirements: allow and facilitate cellular infiltration and in-growth of newly formed tissues by having proper pore structure, size, interconnectivity and total porosity [1]. Scaffolds should also be

biodegradable with a degradation rate matching the new tissue formation rate [1–3]. They should further possess suitable mechanical properties to provide temporary mechanical support; however, increased mechanical properties require dense scaffolds, while enhanced cell in-growth and tissue regeneration require porous scaffolds [4].

The use of a single material to satisfy these numerous requirements is not possible; therefore, composite systems, which combine the advantages of different materials, are more promising [5]. One such class of composites comprises natural polymers and bioceramics to benefit from the flexibility and easy shaping capability of polymers with the higher strength, stiffness, and bioactivity of the bioactive inorganic fillers, thus achieving the best possible mechanical and biological performance [5–9].

Naturally derived biopolymers are mainly proteins (for example collagen, gelatin, zein and silk) and polysaccharides (e.g. starch, alginate, cellulose, chitosan, etc) [1]. Zein, one of the plant proteins currently of interest, is a major storage protein of corn and an alcohol-soluble protein, but insoluble in water. Zein shows a promising potential for tissue engineering and drug delivery applications owing to its availability, good mechanical properties and no immunogenicity compared to animal-derived proteins such as collagen [1, 2, 10–13].

Zein protein has been proven to be biocompatible with endothelial cells of human umbilical veins [14], human liver cells [15], mice fibroblast cells [15], rat bone mesenchymal stem cells [12], human bone marrow stromal cells [13], and human periodontal ligament cells [16]. Thus, zein shows promising potential as a scaffold for TE applications. However, zein lacks bioactive behavior in simulated body fluid (SBF) [11, 17, 18], e.g. the induction of the growth of a hydroxyapatite (HA) phase on the material surface in contact with biological fluids, which is often used to characterize *in vitro* the bone-bonding ability of a material [19].

A characteristic feature of bioactive materials, including bioactive glasses (BGs) and calcium phosphate (CaP) ceramics, is the time-dependent and dynamic interactions that occur at the surface upon contact with biological fluids. The formation of highly reactive carbonated HA layer (HCA) provides the bonding interface with bone as well as soft tissues for special compositions [20]. The bioactivity of BGs is achieved by releasing critical concentrations of biologically active soluble silicon (Si), calcium (Ca), phosphorus (P), and sodium (Na) ions, during BG controlled dissolution at the rate needed for cell proliferation and differentiation [21].

Silver ions (Ag^+) have a well-documented broad antibacterial effect [22–28], which is considered a promising solution to post-implantation bacterial infections, which often complicates wound healing. The incorporation of Ag^+ ions in BGs has been the subject

of considerable research efforts [23–26, 29–33]. In this study, we hypothesize that the addition of Ag^+ ions into BG and the incorporation of this BG into zein scaffolds will benefit from the favorable biocompatibility and mechanical properties of zein, the bioactivity of the glass, and the antibacterial action of silver. Therefore, the aim of the current study is to investigate the *in vitro* antibacterial activity, biocompatibility, bioactivity and compressive strength of a new family of zein scaffolds containing silver-doped bioactive glass.

2. Materials and methods

2.1. Bioactive glass powder preparation

Undoped (BG) and 5 wt% Ag-doped (Ag-BG) were prepared via the sol-gel process according to the method described by El-Kady *et al* [24] with some modifications. 5 wt% Ag-doped BG with the composition (wt%) of 58 SiO_2 , 28 CaO , 9 P_2O_5 , and 5 Ag_2O was prepared by sequential mixing of tetraethyl orthosilicate (TEOS) (Sigma-Aldrich, Germany), distilled water, and 2 M nitric acid (VWR Chemicals, Germany) in ethanol. The mixture was stirred for 60 min at room temperature under continuous magnetic stirring to allow the acid hydrolysis of TEOS. Followed by the sequential addition of triethyl phosphate (TEP) (Merck, Germany), calcium nitrate tetrahydrate $\text{Ca}(\text{NO}_3)_2 \cdot 4\text{H}_2\text{O}$ (Sigma-Aldrich, Germany) and silver nitrate AgNO_3 (VWR Chemicals, Germany), allowing 60 min for each chemical to react. After the final addition, the mixture was stirred for 60 min to allow the completion of hydrolysis. 2 M ammonia solution (a gelation catalyst) was added dropwise to the mixture while vigorously stirring. Finally, the resulting gel was dried at 60 °C for one day. The dried gel powders were calcined at 700 °C for 2 h at a heating rate of 2 °C min^{-1} .

2.2. Fabrication of zein scaffolds

A particle leaching process was employed using sodium chloride (NaCl) as porogen. For fabrication of pure zein scaffolds, zein powder (Sigma-Aldrich, Germany) was mixed with NaCl particles (100–125 μm) at a ratio of 1:2 (zein:NaCl). For fabrication of the zein-BG scaffolds, 20 wt% of the prepared sol-gel-BGs was added to the zein and NaCl mixture. The mixture was compressed into pellets (10 mm diameter, 6.5 mm height for bioactivity and mechanical tests/10 mm diameter, 2.35 mm height for antibacterial and cell culture tests), using an electrohydraulic pressing device applying a load of 2×10^4 Pa. The pellets were salt-leached in a hot water bath at 80 °C for 2 h under magnetic stirring. Later, the scaffolds were washed in distilled water, frozen for 24 h at –20 °C and afterwards freeze-dried.

2.3. Scaffolds morphology, microstructure, and Fourier transform infrared (FTIR) analysis

Characterization of the scaffolds morphology and microstructure was performed using high resolution scanning electron microscopy (SEM, Auriga, Zeiss, Germany). The prepared scaffolds were fixed to SEM sample holders, using a conductive silver adhesive paste and Au-sputter coated at a current of 20 mA for 40 s. Chemical structure analysis was performed using Fourier transform infrared spectroscopy (FTIR, IRAffinity-1S Fourier Transform Infrared Spectrophotometer, SHIMADZU, Japan).

2.4. *In vitro* bioactivity of scaffolds

The *in vitro* HA forming ability of the prepared scaffolds was investigated. Each scaffold was placed in 50 ml Kokubo simulated body fluid (SBF) [19] in airtight polyethylene bottles and placed in a shaking incubator at 37 °C and 90 rpm. At 7 and 14 days, samples were removed from SBF, washed gently with distilled water to stop any further reactions, and dried at 60 °C for 24 h. The microstructure of formed HA was observed by SEM; chemical structure analysis was performed by FTIR.

2.5. Antibacterial tests

The antibacterial activity of the Ag-doped BG-containing scaffolds, using undoped BG-containing scaffolds and pure zein scaffolds as control, against *Escherichia coli* (*E. coli*) and *Staphylococcus aureus* (*S. aureus*) was investigated by the disc diffusion method (BSAC Disc Diffusion Method for Antimicrobial Susceptibility Testing, Version 4, 2005) [34]. Luria broth (LB) (Luria/Miller) agar plates were inoculated with a standardized culture of *S. aureus* (NCTC 6571) and *E. coli* (NCTC 10418), 20 μ l inoculum was spread evenly over the entire surface of the plate and left to dry for a few minutes before placing the scaffolds. Scaffold discs of 10 mm diameter and 3–4 mm thickness ($n = 8$) were then applied to the surface of agar plates; these plates were incubated for 24 h at 37 °C. After 24 h, the formation of clear zones of inhibition around the scaffolds, if any, was observed.

2.6. *In vitro* biocompatibility tests

The human osteosarcoma cell line MG-63 (Sigma-Aldrich) was used for *in vitro* cell culturing. Cells were cultured in Dulbecco's modified eagle medium (DMEM) (Thermo Fisher Scientific, Germany), supplemented with 10 vol% of fetal bovine serum (Sigma-Aldrich, Germany) and 1 vol% of penicillin-streptomycin (Gibco, Thermo Scientific™, Germany) and incubated at 37 °C, 5% CO₂, and 95% humidity until confluence.

Each of the three scaffold groups (pure zein, zein:BG and zein:Ag-BG,) was placed in a 24-well plate; disinfection was done for one hour by ultraviolet (UV) light, then washed with sterile Dulbecco's phosphate-

buffered saline (Thermo Fisher Scientific, Germany) and preconditioned in culture medium for two days. Scaffolds were seeded with 1 ml of cell suspension containing 100 000 cells and culture medium was changed twice a week.

2.6.1. Cell viability

At predetermined time points (1, 3, 7, and 14 days), MG-63 cell viability was measured using WST-8 cell counting kit-8 (CKK-8, Sigma-Aldrich, Germany). To avoid color changes due to pH fluctuations, which can affect result accuracy, DMEM without phenol red was used (Sigma-Aldrich, Germany). At each time point, the medium was removed, and the scaffolds with cells were washed with phosphate buffered saline (PBS). After PBS removal, culture medium containing 1 vol% WST-8 was added to each well and incubated at 37 °C for 4 h. Then, the supernatant from each sample was collected and transferred to a 96-well plate (100 μ l in each well). The absorbance was measured at 450 nm using a microplate reader (PHOmo, Autobio Labtec Instruments). The WST-8 assay was conducted in triplicate.

2.6.2. Alkaline phosphatase (ALP) activity

The specific ALP enzyme activity assay can be used as a simple marker for osteogenic differentiation. MG-63 cells were seeded on the three scaffold groups (pure zein, zein:BG, zein:Ag-BG) under the same culture condition as described before. ALP enzyme activity of the cells on the scaffolds was measured at different time points (1, 3, 7, and 14 days).

At each time point, cells on the scaffolds were lysed with 1 ml cell lysis buffer containing 20 mM TRIS buffered solution (VWR Chemicals, Germany), 0.1 wt% Triton X-100 (AMRESCO, USA), 1 mM MgCl₂, and 0.1 mM ZnCl₂ (Sigma-Aldrich, Germany). The lysates were collected and centrifuged, 250 μ l of the supernatant was added to 100 μ l of ALP buffer solution (0.1 M Tris, 2 mM MgCl₂ and 9 mM p-NPP (Sigma-Aldrich, Germany), pH = 9.8) and incubated at 37 °C for 4.5 h. The reaction was stopped by adding 650 μ l of 1 M NaOH, and absorbance was measured spectrometrically at 405 and 690 nm (background absorbance). The specific ALP activity was calculated with respect to the incubation time and the total protein content of the cell lysates. The total protein content was measured by Bradford reagent (Sigma-Aldrich, Germany). The specific ALP activity assay was conducted in triplicate.

2.6.3. Mineralization assay

Alizarin red S staining was used for qualitative evaluation of the extracellular mineralization, CaP mineral nodule formation. Calcium forms an Alizarin Red S-calcium complex in a chelation process, and the formed calcium deposits have an orange-red color. Calcium deposits are an indication of successful *in vitro* bone formation [35]. At day 14, the medium

was removed and the samples were washed with PBS, fixed in 70% ethanol, and stained with 40 mM Alizarin Red S (Sigma-Aldrich, Germany) at pH 4.2 for 10 min. Stained samples were rinsed with Nanopure water followed by a 15 min wash with PBS (to remove nonspecific stain, not associated with calcium mineral deposits). Stained samples were imaged for qualitative analysis using a stereomicroscope (Stemi 508 Stereo Microscope, Zeiss, Germany) checking for any orange-red colored deposits. The mineralization assay was conducted in duplicate.

2.7. Compressive strength

To evaluate the potential of zein and zein-BG scaffolds for bone tissue engineering applications, the compressive strength of the three scaffold groups (five replicates per group) was measured. Cylindrical scaffolds, 10 mm in diameter and 10 mm height [36–38], were subjected to uniaxial compression testing (Z050, Zwick Roell, Germany) at a crosshead speed of 1 mm min⁻¹; a preload of 0.1 N and maximum applied force of 1 kN until densification of the specimens occurred.

2.8. Porosity measurement

Interconnected porosity (ϕ_c) of the prepared scaffolds was measured using helium injection at 1.2 bar pressure using a gas pycnometer (Ultrapyc 1200e Helium Pycnometer; Quantachrome Instruments, USA). The bulk volume and dry weight of six replicates from each of the scaffolds groups were measured using a precision caliper (0.01 mm precision) and an electronic balance (0.1 mg precision) to calculate the bulk density of the samples (ρ_b). The true volume (v_t) of each sample was measured using the helium pycnometer to calculate the true (skeletal) density of the samples (ρ_t).

Three measurements were taken for each sample and the final arithmetic mean was then calculated and used in further calculations. The interconnected porosity (ϕ_{He}) was calculated using the following equation [39, 40]:

$$\phi_c = 100 \times \frac{(\rho_b - \rho_t)}{\rho_b}$$

2.9. Statistical analysis

All data were expressed as mean \pm standard deviation. The data were checked using the Shapiro–Wilk test for normal distribution. For normally distributed variables, comparison between the mean of the different materials was carried out using parametric one-way analysis of variance (ANOVA) with a Tukey's post hoc multiple comparison of the mean. Non-normally distributed data were tested using non-parametric Kruskal–Wallis test with Mann–Whitney U test post hoc for pairwise comparisons. A p -

value ≤ 0.05 was considered statistically significant. All tests were two-tailed in diameter.

3. Results

3.1. Morphology and microstructure of scaffolds

SEM micrographs of pure zein, zein:BG, and zein:Ag-BG (figure 1) show that all the different scaffold groups are porous. SEM as 2D pore structure analysis method shows that the scaffolds had a wide range of pore diameter with large-sized pores in the range of 100 μ m, medium-sized pores of 50 μ m, and small-sized pores, which are nano-sized in diameter found in the scaffold struts. In zein scaffolds containing the sol-gel-derived BGs (BG and Ag-BG), the added BG powder is not homogeneously distributed within the zein scaffolds; instead, they are aggregated as clusters with a distinct interface between the zein and the added BGs (figures 1(b.2) and (c.2)).

3.2. FTIR spectra analysis

FTIR spectra of pure zein scaffolds (figure 2) show the three characteristic amide peaks for zein protein at around 1630, 1520, and 1230 cm⁻¹, which correspond to amide I, amide II, and amide III, respectively [1, 11]. Zein:BG scaffolds spectra (the upper two spectra in figure 2) show additional peaks characteristic of SiO₂-based glasses, which are presented as three main vibrational modes of the Si–O–Si groups in the region between 400 and 1300 cm⁻¹ [41–43]. Two additional peaks of the phosphate group (PO₄³⁻) are observed at around 565 and 601 cm⁻¹ [41, 42].

3.3. In vitro bioactivity of scaffolds

SEM micrographs of pure zein scaffolds incubated in SBF (figure 3) show no HA formation on the surface of zein, neither after 7 nor 14 days. This result was also confirmed by the FTIR spectral analysis of incubated zein scaffolds, which show no change in peaks compared to the as-prepared scaffolds (figure 4(a)).

On the other hand, SEM micrographs of zein scaffolds containing the sol-gel-derived BGs (zein:BG and zein:Ag-BG scaffolds) show the formation of rounded shaped HA crystals (figure 3). It is observed that the formed HA crystals do not homogeneously cover the entire scaffold surface; however, they grow in the form of clusters only on the surface of BG leading to a distinct interface between the formed HA crystals and the adjacent zein surface. FTIR spectral analysis (figures 4(b) and (c)) shows the presence of new peaks characteristic of HA formation demonstrated by the increasing intensity of the P–O vibrational band, the appearance of a new carbonate (CO₃²⁻) peak at around 875 cm⁻¹ and a weak silanol peak near 960 cm⁻¹.

3.4. In vitro antibacterial activity

The results of the disc diffusion assay indicated that only zein scaffolds containing Ag-BG had positive

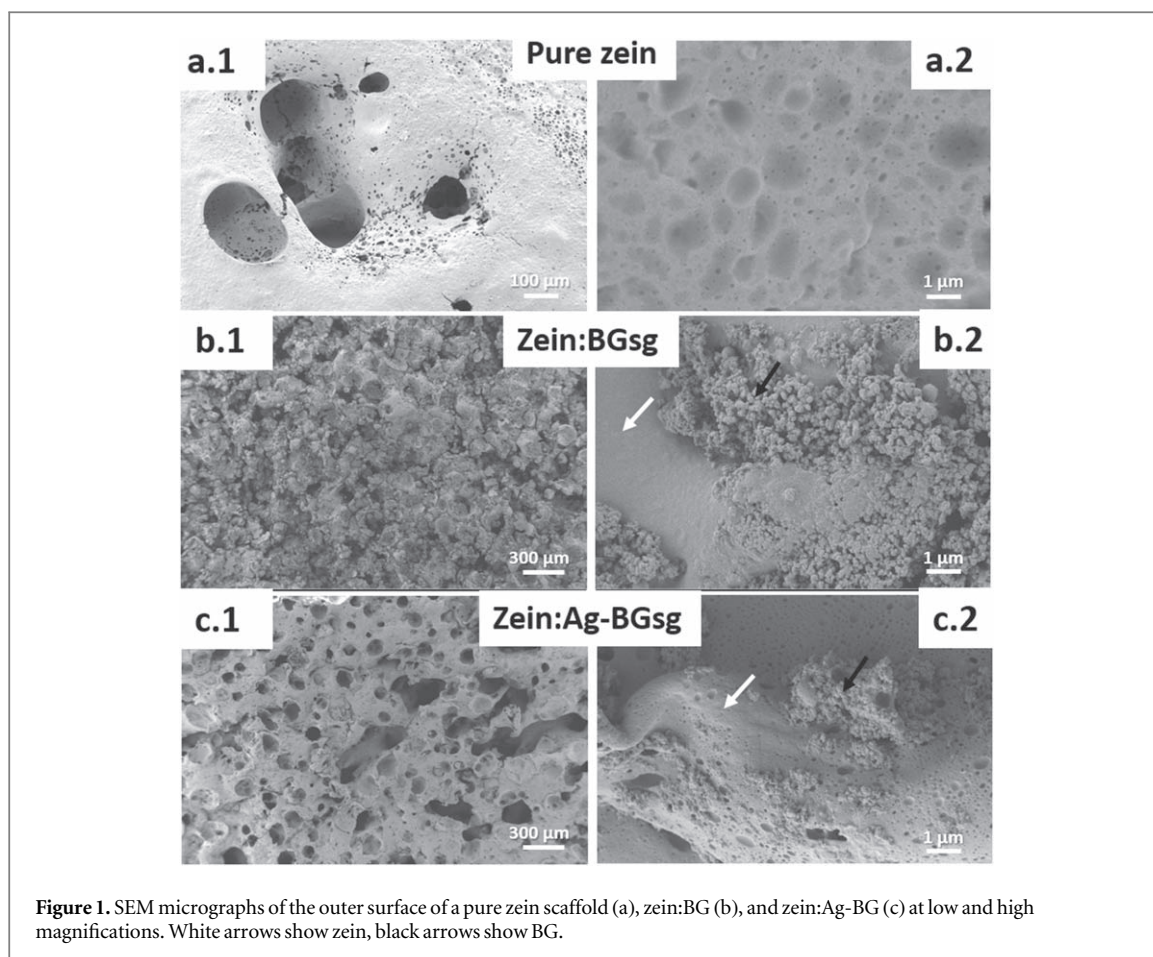


Figure 1. SEM micrographs of the outer surface of a pure zein scaffold (a), zein:BG (b), and zein:Ag-BG (c) at low and high magnifications. White arrows show zein, black arrows show BG.

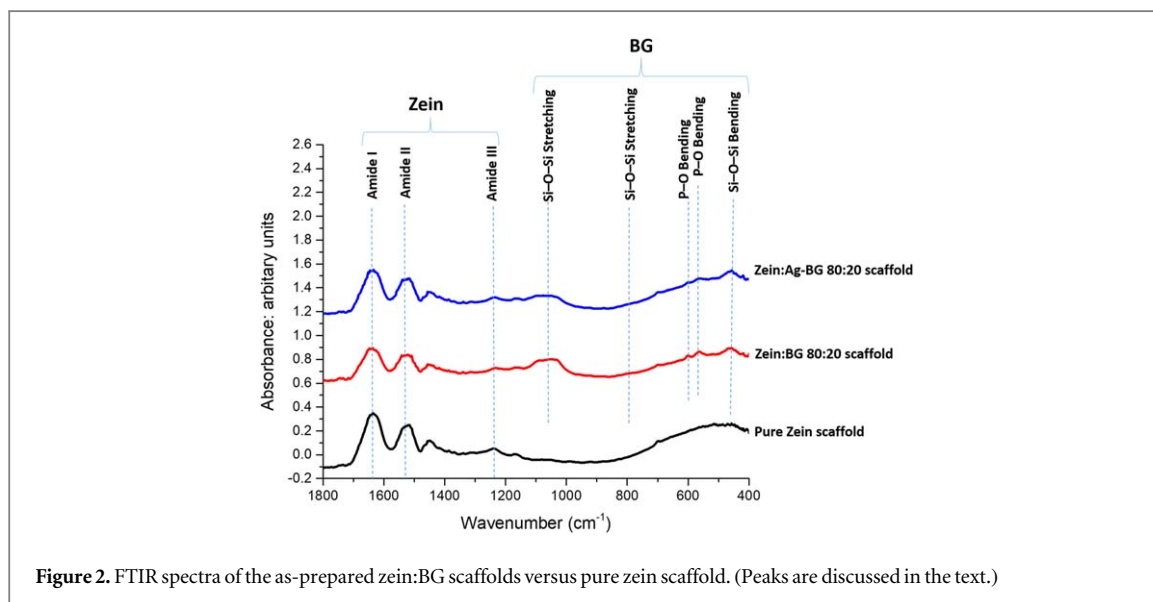


Figure 2. FTIR spectra of the as-prepared zein:BG scaffolds versus pure zein scaffold. (Peaks are discussed in the text.)

antibacterial activity against *E. coli* and *S. aureus* as indicated by the formation of clear zones of inhibition around them (figure 5). However, other scaffold groups showed no antibacterial effect with absence of inhibition zone formation as evident by the ability of bacteria to grow around them.

3.5. *In vitro* biocompatibility tests

3.5.1. Cell viability

Data from the WST-8 assay is shown in figure 6. At all-time points, zein:BG showed the highest mean cell viability. At day 1, 3, and 7, zein:BG scaffold groups showed the highest mean cell viability, which was significantly higher than the value for zein:Ag-BG ($p \leq 0.05$), while it showed no significant difference compared to the pure zein scaffolds. At day 14, the

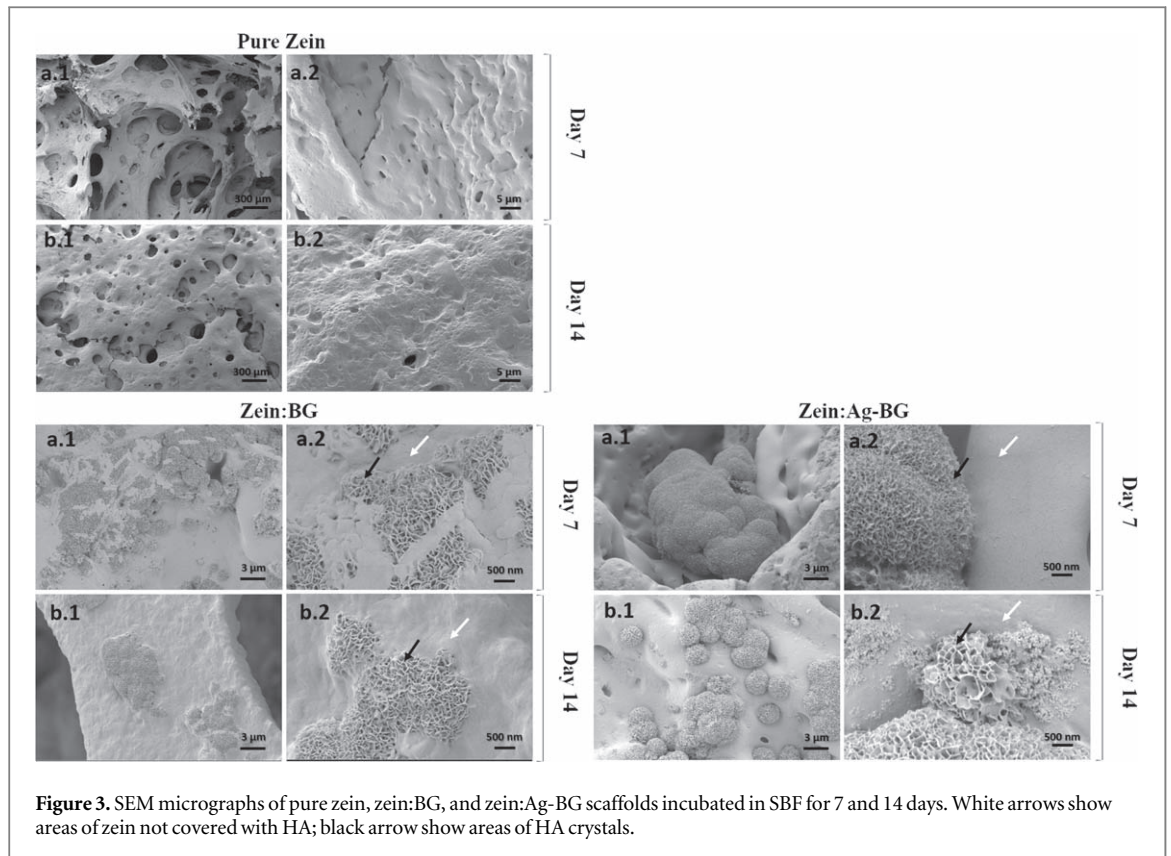


Figure 3. SEM micrographs of pure zein, zein:BG, and zein:Ag-BG scaffolds incubated in SBF for 7 and 14 days. White arrows show areas of zein not covered with HA; black arrow show areas of HA crystals.

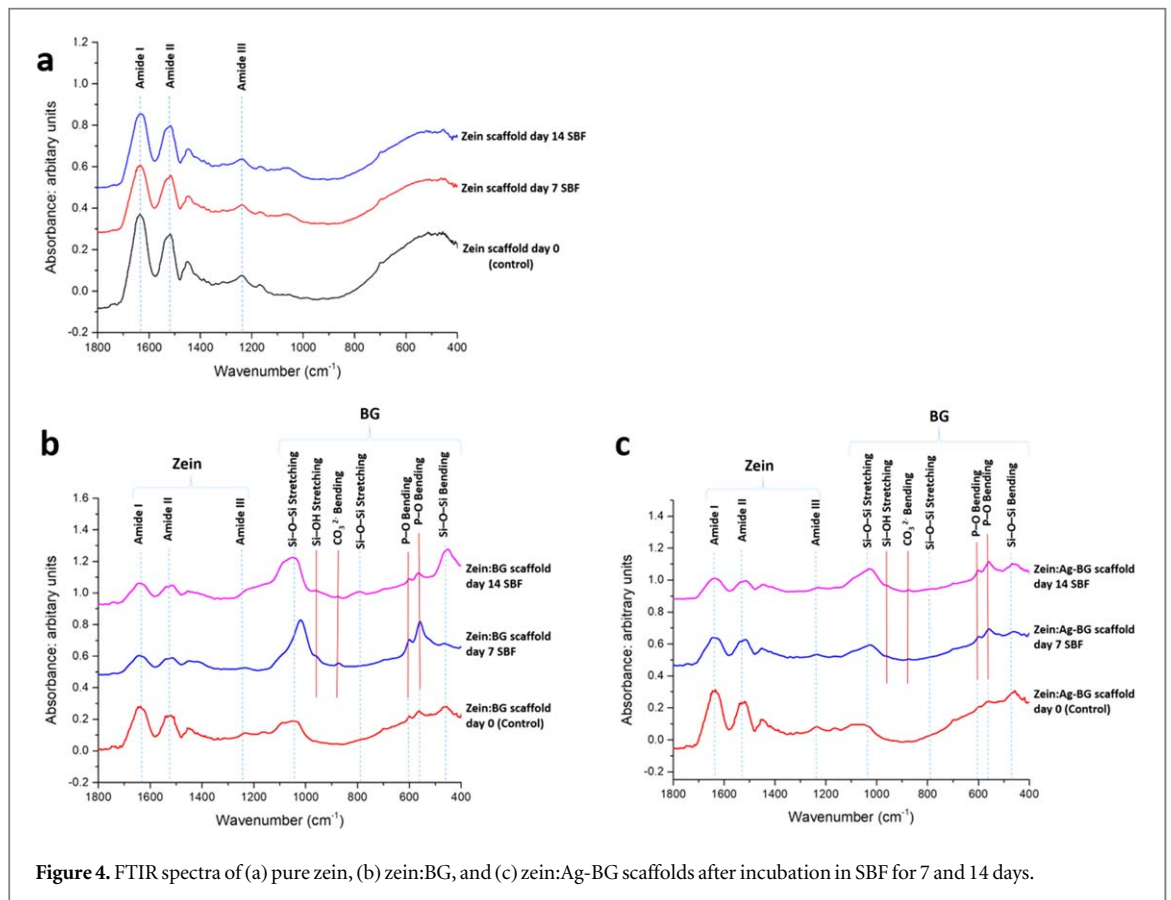


Figure 4. FTIR spectra of (a) pure zein, (b) zein:BG, and (c) zein:Ag-BG scaffolds after incubation in SBF for 7 and 14 days.

zein:BG scaffold exhibited the highest mean value among all groups.

Results showed significant statistical changes in the MG-63 cell count within each of the zein, zein:BG, and zein:Ag-BG groups at the different time points.

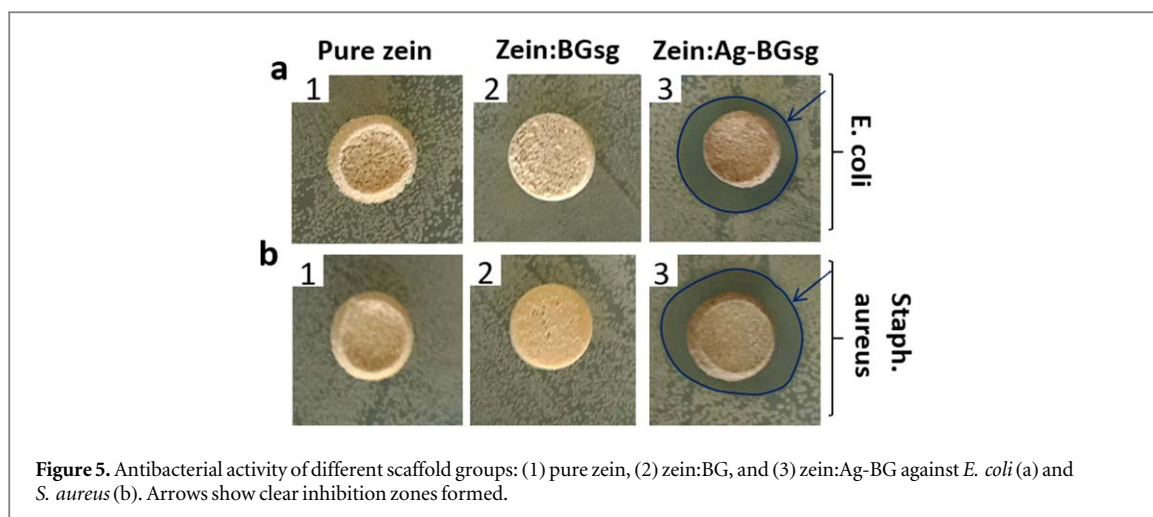


Figure 5. Antibacterial activity of different scaffold groups: (1) pure zein, (2) zein:BG, and (3) zein:Ag-BG against *E. coli* (a) and *S. aureus* (b). Arrows show clear inhibition zones formed.

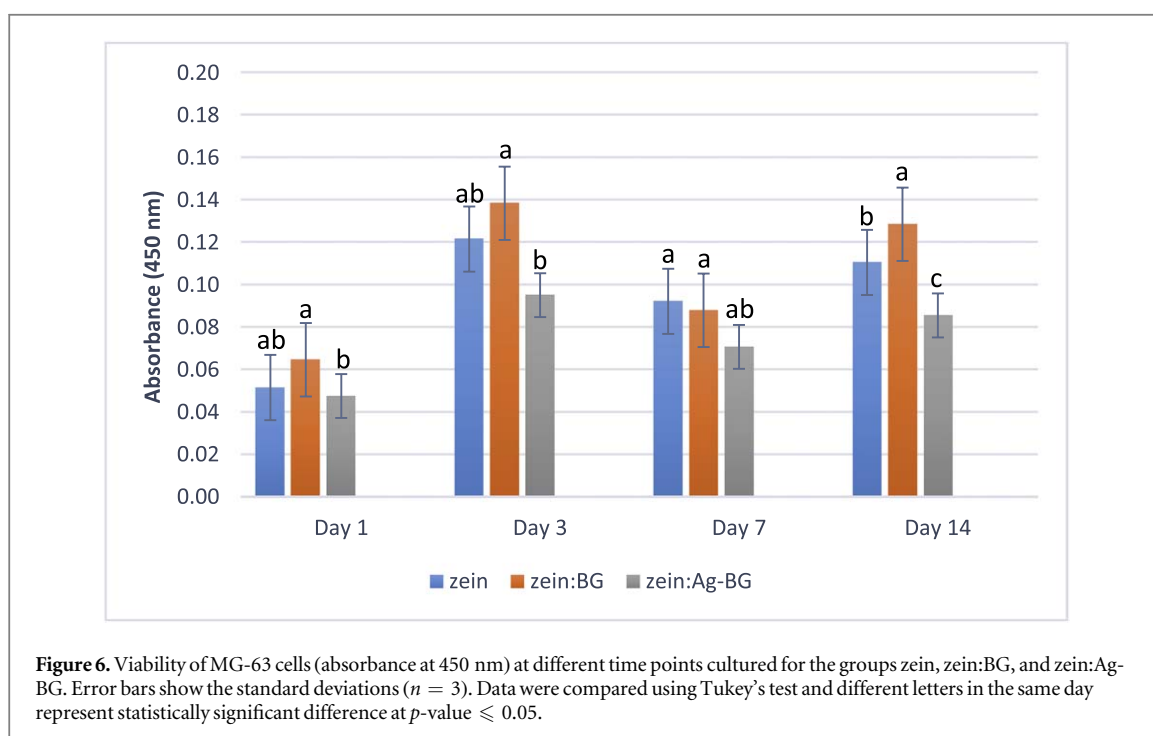


Figure 6. Viability of MG-63 cells (absorbance at 450 nm) at different time points cultured for the groups zein, zein:BG, and zein:Ag-BG. Error bars show the standard deviations ($n = 3$). Data were compared using Tukey's test and different letters in the same day represent statistically significant difference at p -value ≤ 0.05 .

3.5.2. Specific ALP activity

Specific ALP enzyme activity assay revealed that zein:BG scaffolds show no significant difference in the specific ALP activity compared to other groups at most of the time points (day 1, 3, and 14) (figure 7). At day 7, the zein group shows the highest specific ALP activity among all groups ($p \leq 0.05$). The results indicate significant changes in specific ALP activity of MG-63 cells cultured on the zein and zein:BG groups at different time points.

The total protein content of the cell lysates (supplementary information S1 is available online at stacks.iop.org/BMM/13/065006/mmedia) showed no significant difference at day 1 of culture. At days 3, 7 and 14, the zein:BG scaffold group showed the significantly highest values, while the pure zein group showed statistically lower protein content than the two composite scaffold groups.

3.5.3. Mineralization assay

After 14 days of culture, more intense orange-red color staining was observed on zein:BG scaffolds (figure 8(b)) compared to pure zein (figure 8(a)) and zein:Ag-BG (figure 8(c)) scaffolds.

3.6. Compressive strength

The mean compressive strength values showed no significant difference between the pure zein scaffolds and the composite scaffolds containing 20 wt% undoped and Ag-doped BG (table 1).

On the other hand, composite scaffolds containing 10 wt% Ag-doped BG showed significantly higher compressive strength than the pure zein group (supplementary information S2).

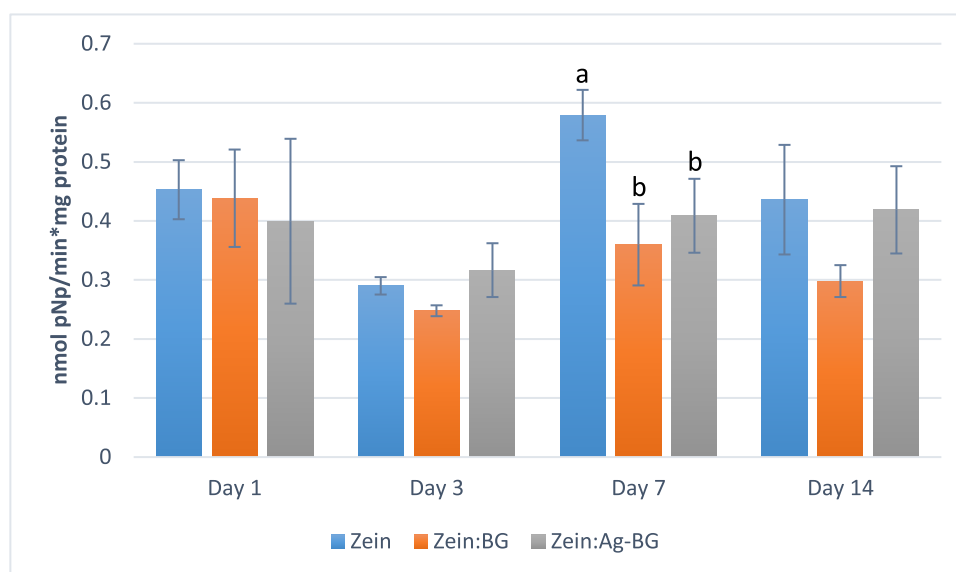


Figure 7. Specific ALP activity of MG-63 cells at different time points cultured on zein, zein:BG, and zein:Ag-BG scaffolds. Error bars show the standard deviations ($n = 3$). Data were compared using Tukey's test and different letters in the same day represent statistically significant difference at p -value ≤ 0.05 .

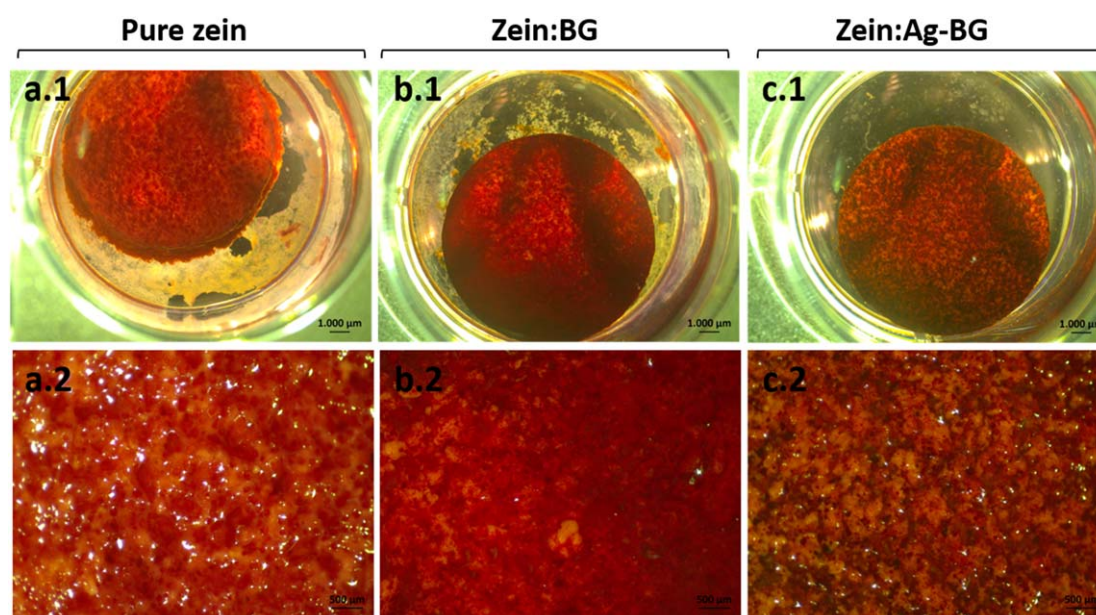


Figure 8. Alizarin red S staining of MG-63 cells cultured on pure zein (a), zein:BG (b), and zein:Ag-BG (c) scaffolds after 14 days.

Table 1. Compressive strength values of the three scaffold groups. Data are represented as means (\pm SD) and compared using one-way ANOVA test ($n = 5$).

	Compressive strength (MPa)
Pure zein	5 ± 2
Zein:BG	5 ± 1
Zein:Ag-BG	5 ± 2
p -value	0.840

3.7. Porosity measurement

Statistically significant differences in mean interconnected porosity were found among the different groups ($p \leq 0.05$). Zein:BG scaffolds exhibited the highest mean porosity while the total porosity of pure zein was statistically lower than that in the other two groups (table 2).

4. Discussion

Composite scaffolds combining natural polymers and bioceramics are promising candidates for hard tissue

Table 2. Interconnected porosity (ϕ_c) (in %) of different scaffolds. Data are represented as means (\pm SD) and compared using Tukey's test ($n = 6$).

	Interconnected porosity (%)
Pure zein	67 ± 2^c
Zein:BG	85 ± 3^a
Zein:Ag-BG	80 ± 2^b
<i>p</i> -value	$<0.0001^*$

Note. Different letters represent statistically significant differences at p -value ≤ 0.05 .

*Highly statistical significance at p -value ≤ 0.001 .

engineering. This is achieved by providing the best possible mechanical and biological performance and by combining the advantages of polymers, such as flexibility and easy shaping, with the higher strength, stiffness, and bioactivity of the bioactive inorganic fillers. Zein is one of the naturally-derived polymers currently of interest, based on its biocompatibility, suitable mechanical properties and availability, while bioactive glasses are well-known for their good bone-forming ability. The current study aimed at investigating the *in vitro* antibacterial properties, biocompatibility, bioactivity and compressive strength of novel 3D nanocomposite zein scaffolds containing undoped and silver-doped bioactive glass nanoparticles in comparison to pure zein scaffolds.

SEM micrographs showed the formation of zein and composite zein:BG scaffolds with highly interconnected porous networks (figure 1). The existence of macro and micro-sized pores was evident with the characteristic presence of micropores in the walls of the macropores, which was previously reported for zein scaffolds fabricated by the salt-leaching method [11, 12, 16, 17]. The SEM micrographs showed that the sol-gel-derived BG particles are not fully embedded in zein (figures 1(b.2)). This may be attributed to the hydrophilicity of the sol-gel-derived glasses and the hydrophobicity of zein [17].

FTIR spectral analysis of the as-prepared scaffolds (figure 2) showed the characteristic bands of zein in the pure zein scaffold. The amide I peak is associated with stretching of carbonyl (C=O) of the amide groups. The amide II peak corresponds to the angular deformation vibrations of the N-H bond. Finally, the amide III band reflects the axial deformation vibrations of the C-N bond [1, 11]. In zein:BG scaffolds, both bands characteristic of zein and silicate BG were observed. Silicate-based glasses are characterized by the three main vibrational modes of the Si-O-Si groups (between 400 and 1300 cm^{-1}) [41–43]. The broad band located in the range of 1000–1200 cm^{-1} is associated with Si-O-Si asymmetric stretching vibration, whereas the band observed around 800 cm^{-1} corresponds to the Si-O-S symmetric stretching

vibration. In addition, the band located around 450 cm^{-1} is identified as the Si-O-Si bending mode [41–43]. Vibrational peaks of the phosphate group observed at 565 and 601 cm^{-1} are associated with the P-O asymmetric bending mode in bioactive glasses containing phosphate groups [41, 42]. However, no new peaks were observed, which indicate the absence of chemical interaction between zein and the incorporated BG particles.

It is well-known that *in vitro* bioactivity (or bioactivity) may be related to bone-bonding ability *in vivo*, considering that bioactive materials should provide a favorable environment for osteoblasts to proliferate, differentiate and produce apatite and collagen [19, 44]. The *in vitro* apatite-forming ability of biomaterials is commonly evaluated by incubating the samples in SBF to detect HCA layer formation [19]. The formation of HCA involves several stages: including an initial rapid exchange of alkali ions with hydrogen ions in the body fluids (or SBF), followed by silica network dissolution and formation of Si-OH (silanol) bonds, which is followed by silica gel polymerization, which enhances HA crystals nucleation, and final crystallization of HCA layer through the incorporation of hydroxyls (OH^-) and carbonate (CO_3^{2-}) from the solution [45].

After incubation of pure zein scaffolds in SBF, SEM micrographs showed lack of HA crystal formation, even after 14 days of incubation in SBF (figure 3). These findings were confirmed by FTIR analysis, where no new peaks were observed compared to the as-prepared scaffolds (figure 4(a)), which indicates that zein lacks bioactive behavior in SBF [11, 17, 18]. The lack of mineralization of zein upon incubation in SBF could be attributed to its hydrophobicity [11], the lack of relevant elements (Ca, P) and the slow dissolution of zein in SBF, which hinders the formation of HA [11, 18].

Zein scaffolds containing both undoped and silver-doped sol-gel BGs showed evidence of mineralization and formation of the characteristic morphology of HA crystals at both 7 and 14 days (figure 3). Bioactivity of the incubated scaffolds was confirmed by FTIR analysis, which showed the existence of new peaks characteristic of HCA layer formation, as shown by the increasing intensity of the P-O vibrational band (565 and 601 cm^{-1}) [42, 43]. In addition, the new carbonate (CO_3^{2-}) peak observed at around 875 cm^{-1} suggests the formation of HCA, which resembles the mineralized inorganic component of bone [42, 46, 47] as well as the weak silanol peak observed near 960 cm^{-1} , is related to the bioactive surface reactions occurring in contact with SBF [41, 42] (figures 4(b) + (c)).

It is evident from SEM micrographs that newly formed HA crystals have grown on top of BG particles only, which confirms that the added BG is the only constituent responsible for the bioactive behavior of the composite scaffolds (figure 3). The mechanism of

HA formation is suggested to be based on the rapid initial release of Ca^{2+} from the BG, coupled with an increase in local pH, which attacks the silica glass network and subsequent formation of silica-rich layer [48, 49]. This layer enhances the formation of the HA nuclei crystallization from the high concentration of Ca^{2+} and PO_4^{3-} present [47].

Disc diffusion assay results showed that only zein:Ag-BG scaffolds were antibacterial against *E. coli* and *S. aureus* (figure 5). The antibacterial activity of these scaffolds could be attributed to the leaching out of Ag^+ ions from the glass matrix. The antibacterial activity of silver nanoparticles is well-documented [22–28, 50], and the release of silver ions from the scaffolds is a diffusion-controlled mechanism and depends on the BG content of the scaffolds [48]. The addition of Ag-doped BG nanoparticles as filler in these nanocomposite scaffolds is aimed primarily at imparting antibacterial activity to the scaffolds through releasing antibacterial silver ions during their degradation. Scaffolds containing lower Ag-doped BG ratio (10 wt%), failed to show antibacterial effect with absence of inhibition zone formation (data not shown), which could be due to the lower amount of silver ions released, incapable of inhibiting bacterial growth.

Cellular attachment and interaction with the scaffold surfaces are essential processes for cell proliferation, differentiation and their normal functions [51]. Thus, MG-63 cell viability, differentiation and mineralization were assessed using WST-8, specific ALP activity, and Alizarin Red S staining assays, respectively.

Zein protein has been proven to be biocompatible in previous *in vitro* and *in vivo* investigations [3, 12–16, 52, 53]. In the current study, scaffolds were preconditioned in culture medium for two days before seeding the cells; this was performed because BGs, particularly the sol-gel derived, release a high initial burst concentration of Ca ions following their immersion in physiological fluids with a pH rise in the first three days [54]. Such burst Ca release and pH change have been reported to adversely affect cell attachment and growth [35, 54, 55].

WST-8 assay at day 1, 3, 7, and 14 of culture showed the ability of MG-63 cells to proliferate on the pure zein scaffolds and zein scaffolds containing sol-gel-derived BGs (figure 6). At day 14, zein:BG scaffolds exhibited the highest mean cell count among all groups. However, both pure zein and zein:Ag-BG were proven suitable for supporting MG-63 cell viability and growth and had no negative effect on proliferation. A possible explanation of the enhanced cellular proliferation with zein:BG scaffolds would be the markedly higher specific surface area of the sol-gel-derived glasses with subsequent higher dissolution and ion release rate and higher bioactivity. The higher specific surface area could provide more sites for adsorption of proteins and growth factors, enhancing the subsequent cell attachment and proliferation. In

addition, the effect of Si species released during BG dissolution on enhancing osteoblast proliferation and activity, e.g. gene expression, have been previously reported [51, 56, 57]. The lower proliferation of MG-63 on zein:Ag-BG scaffolds could be induced by the release of Ag^+ ions, which could have a possible slight cytotoxic effect in such static culture conditions. Further studies using dynamic culture conditions, which would provide better nutrient and mass transfer, could show different cellular response.

Specific ALP is the most widely recognized marker of osteoblastic differentiation and activity [51, 58–60]. ALP is an essential enzyme for mineralization, associated with the plasma membrane of osteoblasts, which is present in high levels in matrix vesicles (MV) observed in developing bone [58, 61]. The differentiation behavior and activity of MG-63 cells on the scaffolds were investigated using specific ALP activity assay. Results showed that ALP activity followed a different trend to the proliferation behavior observed with WST-8 assay, where no statistically significant difference in specific ALP activity was observed among the investigated groups at most time points, except for day 7 (figure 7). An abrupt decrease in ALP activity on zein:BG scaffolds was observed after day 1, although cells cultured on the zein:BG group showed significantly higher total protein content (at days 3, 7 and 14), which indicates higher cellular proliferation compared to pure zein and zein:Ag-BG groups (supplementary information S1). Similar findings were reported by *Sadat-Shojai et al* [62], who used mouse pre-osteoblastic MC3T3-E1 cells, and *Nuttelman et al* [63], who used human mesenchymal stem cells, where ALP activity decreased with progressive increase in mineralization.

A possible explanation of the decreased ALP activity with progressive mineralization was proposed by *Genge et al* [61], who reported that a loss in ALP activity (up to 65%–70%) may accompany Ca^{2+} accumulation during MV-mediated mineralization. Such decline in ALP activity was suggested to be the result of the combined action of several factors, including loss of enzyme activity through adsorption of the mineral to the enzyme. Other factors include loss of zinc (Zn^{2+}) and magnesium (Mg^{2+}) metal ions from the active site of the enzyme. ALP enzyme is a metalloenzyme with both Zn^{2+} and Mg^{2+} at its active site, their loss might result in irreversible denaturation of the enzyme during mineralization [61].

Osteoblast differentiation either *in vitro* or *in vivo* can be characterized in three stages: cell proliferation, matrix maturation, and matrix mineralization [64]. Alizarin red S staining assay used to evaluate extracellular mineralization after 14 days of culture showed mineral deposition on the three scaffold groups (figure 8). However, pure zein (figure 8(a)) and zein:Ag-BG (figure 8(c)) groups showed little mineral deposition, as indicated by nodules of orange-red color formed (Alizarin red S positive nodules), while

zein:BG (figure 8(b)) showed markedly abundant heavily stained Alizarin Red S positive nodules, suggesting a higher extent of mineralization. The higher MG-63 mineralization on zein:BG scaffolds indicates the higher activity of cells, which suggests the promising potential of these scaffolds for bone tissue engineering [35]. Mineral nodule formation on zein:Ag-BG scaffolds was also evident, although to a less extent than that formed on zein:BG scaffolds. The lower mineralization activity of MG-63 on zein:Ag-BG scaffolds could be induced by the release of Ag^+ ions, as discussed earlier.

Among the requirements of BTE scaffolds, mechanical properties are of prime importance; the implanted scaffold should exhibit adequate mechanical stability enabling a suitable environment for new bone tissue formation [65]. BTE scaffolds should provide and maintain structural support during cellular proliferation and subsequent mineralization, leaving space for new bone tissue growth during scaffold degradation [3]. The compressive strength values of the investigated groups (table 1) were in the range of those of cancellous bone (2–12 MPa for compressive strength) [12], which indicates their suitability for BTE in non-load bearing areas. There was no significant difference between the compressive strength values of the three fabricated groups, pure zein, zein:BG, and zein:Ag-BG. The addition of sol-gel-derived nano-sized BG (in 20 wt%) did not affect the relatively good mechanical properties of zein scaffolds.

The addition of 10 wt% Ag-doped BG significantly enhanced the compressive strength of the prepared scaffolds, compared to the pure zein scaffolds (supplementary information S2). However, increasing the amount of the added BGs to 20 wt% to impart antibacterial activity to the prepared scaffolds was needed, which resulted in decrease in the mechanical strength of the composite scaffolds. Higher ratios of BG fillers have been often reported to result in a decrease of composite scaffolds compressive strength and stiffness [11, 17]. The interference of the added BG with zein plasticization process during salt-leaching could be the cause for such decrease [17]. However, it is noteworthy that the addition of sol-gel-derived BG (in 20 wt% concentration) in the present study did not affect the relatively good mechanical properties of zein scaffolds.

The interconnected porosity (\varnothing_c) of the prepared pure zein, zein:BG, and zein:Ag-BG scaffolds was analyzed using helium pycnometer. This method was selected among the different methods available for porosity characterization as Archimedes' method is not suitable for the hydrophobic zein polymer [66], and the theoretical gravimetric method necessitates accurate determination of the true density of the scaffold material. The density of zein (1.22 g cm^{-3}) commonly used with this method [17] and in the apparent density method [3, 12, 13, 67] is not an accurate representative of the true zein density after the plasticization

and salt-leaching method which affect the degree of crystallinity of the polymer. Hence, gas pycnometry, using helium as the analysis gas, was used for determination of the open porosity of the prepared scaffolds.

Scaffolds for TE applications require a total porosity of at least 70%, which should be highly interconnected to aid in the delivery of nutrients to the cells and removal of metabolic waste in addition to support tissue in-growth [68]. High pore interconnectivity facilitates uniform cell seeding and migration and allows for nutrients diffusion into and metabolites diffusion out of the TE construct [65]. The measurement of the mean interconnected porosity showed that there was statistically significant difference among the three scaffold groups (table 2).

The porous structure is created during the leaching of the NaCl porogens during the salt-leaching process. The higher mean porosity of the zein:sol-gel-derived groups, compared to pure zein scaffolds, could be attributed to the possible dissolution of some of the BG particles during the leaching process [17]. The higher porosity of zein:BG group compared to the zein:Ag-BG group might be explained by the fact that the BG powder had higher volume/mass ratio (lower density) compared to the Ag-BG powder [69]. As a result, the amount of Ag-BG particles incorporated in zein scaffolds was lower than that of undoped BG, hence, a possible explanation for the lower open porosity of zein:Ag-BG scaffolds is the dissolution of lower amount of Ag-BG than BG.

5. Conclusions

Zein scaffolds containing undoped and Ag-doped sol-gel-derived BG were shown to offer *in vitro* biocompatibility, exhibiting comparable mechanical properties, in addition to providing enhanced *in vitro* bioactive properties. Moreover, addition of Ag-doped sol-gel-derived BG to the zein scaffolds induces additional antibacterial activity against *E. coli* and *S. aureus* microorganisms. Future studies must evaluate these newly prepared scaffolds *in vivo*.

Acknowledgments

The authors would like to thank Professor Bassem Nabawy for his experienced and valuable assistance with the porosity measurement. They also thank Alina Grünwald for her valuable technical assistance with cell culture. Financial support provided by the Egyptian Ministry of Higher Education (MoHE) and the German Academic Exchange Service (DAAD) for Aiah A El-Rashidy is acknowledged.

ORCID iDs

Aiah A El-Rashidy  <https://orcid.org/0000-0002-4475-0837>

Aldo R Boccaccini  <https://orcid.org/0000-0002-7377-2955>

References

- [1] Corradini E, Curti P S, Meniqueti A B, Martins A F, Rubira A F and Muniz E C 2014 Recent advances in food-packing, pharmaceutical and biomedical applications of zein and zein-based materials *Int. J. Mol. Sci.* **15** 22438–70
- [2] Nitta S K and Numata K 2013 Biopolymer-based nanoparticles for drug/gene delivery and tissue engineering *Int. J. Mol. Sci.* **14** 1629–54
- [3] Wang H J, Gong S J, Lin Z X, Fu J X, Xue S T, Huang J C and Wang J Y 2007 *In vivo* biocompatibility and mechanical properties of porous zein scaffolds *Biomaterials* **28** 3952–64
- [4] Hollister S J, Maddox R D and Taboas J M 2002 Optimal design and fabrication of scaffolds to mimic tissue properties and satisfy biological constraints *Biomaterials* **23** 4095–103
- [5] Rezwan K, Chen Q Z, Blaker J J and Boccaccini A R 2006 Biodegradable and bioactive porous polymer/inorganic composite scaffolds for bone tissue engineering *Biomaterials* **27** 3413–31
- [6] Boccaccini A R, Erol M, Stark W J, Mohn D, Hong Z and Mano J F 2010 Polymer/bioactive glass nanocomposites for biomedical applications: a review *Compos. Sci. Technol.* **70** 1764–76
- [7] Lu H H, El-Amin S F, Scott K D and Laurencin C T 2003 Three-dimensional, bioactive, biodegradable, polymer-bioactive glass composite scaffolds with improved mechanical properties support collagen synthesis and mineralization of human osteoblast-like cells *in vitro* *J. Biomed. Mater. Res. A* **64** 465–74
- [8] Bae W-J, Min K-S, Kim J-J, Kim H-W and Kim E-C 2012 Odontogenic responses of human dental pulp cells to collagen/nanobioactive glass nanocomposites *Dent. Mater.* **28** 1271–9
- [9] Miyazaki T, Ishikawa K, Shirotsuki Y and Ohtsuki C 2013 Organic-inorganic composites designed for biomedical applications *Biol. Pharm. Bull.* **36** 1670–5
- [10] Reddy N and Yang Y 2011 Potential of plant proteins for medical applications *Trends Biotechnol.* **29** 490–8
- [11] Naseri S, Hum J, Lepry W C, Miri A K, Nazhat S N and Boccaccini A R 2015 Fabrication and characterization of zein-bioactive glass scaffolds *Bioinspired, Biomim. Nanobiomater.* **4** 73–8
- [12] Gong S, Wang H, Sun Q, Xue S-T and Wang J-Y 2006 Mechanical properties and *in vitro* biocompatibility of porous zein scaffolds *Biomaterials* **27** 3793–9
- [13] Qu Z-H, Wang H-J, Tang T-T, Zhang X-L, Wang J-Y and Dai K-R 2008 Evaluation of the zein/inorganics composite on biocompatibility and osteoblastic differentiation *Acta Biomater.* **4** 1360–8
- [14] Wang H-J, Lin Z-X, Liu X-M, Sheng S-Y and Wang J-Y 2005 Heparin-loaded zein microsphere film and hemocompatibility *J. Control. Release* **105** 120–31
- [15] Dong J, Sun Q and Wang J 2004 Basic study of corn protein, zein, as a biomaterial in tissue engineering, surface morphology and biocompatibility *Biomaterials* **25** 4691–7
- [16] Yan-Zhi X, Jing-Jing W, Chen Y-P, Liu J, Li N and Yang F-Y 2010 The use of zein and Shuanghuangbu for periodontal tissue engineering *Int. J. Oral Sci.* **2** 142–8
- [17] Hum J K 2016 Bioactive glass combined with natural derived proteins as composite materials for the application in bone tissue engineering *PhD Thesis* University of Erlangen-Nuremberg
- [18] Zhou P Y, Xia Y, Wang J, Liang C, Yu L, Tang W, Gu S and Xu S G 2013 Antibacterial properties and bioactivity of HACC- and HACC-zein-modified mesoporous bioactive glass scaffolds *J. Mater. Chem. B* **1** 685–92
- [19] Kokubo T and Takadama H 2006 How useful is SBF in predicting *in vivo* bone bioactivity? *Biomaterials* **27** 2907–15
- [20] Ratner B D, Hoffman A S, Schoen F J and Lemons J E 2012 *Biomaterials Science: An Introduction to Materials in Medicine* 3rd edn (New York: Academic)
- [21] Hench L L 2006 The story of Bioglass® *J. Mater. Sci., Mater. Med.* **17** 967–78
- [22] Kon K and Rai M 2013 Metallic nanoparticles: mechanism of antibacterial action and influencing factors *J. Comp. Clin. Pathol. Res.* **1** 160–74
- [23] Balamurugan A, Balossier G, Laurent-Maquin D, Pina S, Rebelo A H S, Faure J and Ferreira J M F 2008 An *in vitro* biological and anti-bacterial study on a sol-gel derived silver-incorporated bioglass system *Dent. Mater.* **24** 1343–51
- [24] El-Kady A M, Ali A F, Rizk R A and Ahmed M M 2012 Synthesis, characterization and microbiological response of silver doped bioactive glass nanoparticles *Ceram. Int.* **38** 177–88
- [25] Hu G, Xiao L, Tong P, Bi D, Wang H, Ma H, Zhu G and Liu H 2012 Antibacterial hemostatic dressings with nanoporous bioglass containing silver *Int. J. Nanomed.* **7** 2613–20
- [26] Bellantone M, Williams H D and Hench L L 2002 Broad-spectrum bactericidal activity of Ag₂O-doped bioactive glass *Antimicrob. Agents Chemother.* **46** 1940–5
- [27] Mandal A, Meda V, Zhang W J, Farhan K M and Gnanamani A 2012 Synthesis, characterization and comparison of antimicrobial activity of PEG/TritonX-100 capped silver nanoparticles on collagen scaffold *Colloids Surf. B* **90** 191–6
- [28] Cardoso V S et al 2014 Collagen-based silver nanoparticles for biological applications: synthesis and characterization *J. Nanobiotechnol.* **12** 36
- [29] Magyari K, Gruian C, Varga B, Ciceo-Lucacel R, Radu T, Steinhoff H-J, Váró G, Simon V and Baia L 2014 Addressing the optimal silver content in bioactive glass systems in terms of BSA adsorption *J. Mater. Chem. B* **2** 5799–808
- [30] Nezafati N, Moztarzadeh F and Hesarak S 2012 Surface reactivity and *in vitro* biological evaluation of sol gel derived silver/calcium silicophosphate bioactive glass *Biotechnol. Bioprocess Eng.* **17** 746–54
- [31] Gargiulo N, Cusano A M, Causa F, Caputo D and Netti P A 2013 Silver-containing mesoporous bioactive glass with improved antibacterial properties *J. Mater. Sci., Mater. Med.* **24** 2129–35
- [32] Goh Y F, Alshemary A Z, Akram M, Abdul Kadir M R and Hussain R 2014 Bioactive glass: an *in vitro* comparative study of doping with nanoscale copper and silver particles *Int. J. Appl. Glass Sci.* **12** 1–12
- [33] Delben J R J, Pimentel O M, Coelho M B, Candelorio P D, Furini L N, Alencar Dos Santos F, De Vicente F S and Delben A A S T 2009 Synthesis and thermal properties of nanoparticles of bioactive glasses containing silver *J. Therm. Anal. Calorim.* **97** 433–6
- [34] Andrews J M 2005 BSAC standardized disc susceptibility testing method (version 4) *J. Antimicrob. Chemother.* **56** 60–76
- [35] Gough J E, Jones J R and Hench L L 2004 Nodule formation and mineralisation of human primary osteoblasts cultured on a porous bioactive glass scaffold *Biomaterials* **25** 2039–46
- [36] Xu C, Su P, Chen X, Meng Y, Yu W, Xiang A P and Wang Y 2011 Biocompatibility and osteogenesis of biomimetic bioglass-collagen-phosphatidylserine composite scaffolds for bone tissue engineering *Biomaterials* **32** 1051–8
- [37] Fu H, Fu Q, Zhou N, Huang W, Rahaman M N, Wang D and Liu X 2009 *In vitro* evaluation of borate-based bioactive glass scaffolds prepared by a polymer foam replication method *Mater. Sci. Eng. C* **29** 2275–81
- [38] Wang H, Zhao S, Zhou J, Shen Y, Huang W, Zhang C, Rahaman M N and Wang D 2014 Evaluation of borate bioactive glass scaffolds as a controlled delivery system for copper ions in stimulating osteogenesis and angiogenesis in bone healing *J. Mater. Chem. B* **2** 8547–57

- [39] Nabawy B S, Rochette P and Géraud Y 2009 Petrophysical and magnetic pore network anisotropy of some cretaceous sandstone from Tushka Basin, Egypt *Geophys. J. Int.* **177** 43–61
- [40] Nabawy B S 2014 Estimating porosity and permeability using digital image analysis (DIA) technique for highly porous sandstones *Arab. J. Geosci.* **7** 889–98
- [41] Aguiar H, Serra J, González P and León B 2009 Structural study of sol-gel silicate glasses by IR and Raman spectroscopies *J. Non-Cryst. Solids* **355** 475–80
- [42] Zheng K, Solodovnyk A, Li W, Goudouri O M, Stähli C, Nazhat S N and Boccaccini A R 2015 Aging time and temperature effects on the structure and bioactivity of gel-derived 45S5 glass-ceramics *J. Am. Ceram. Soc.* **98** 30–8
- [43] Kozon D, Zheng K, Boccardi E, Liu Y, Liverani L and Boccaccini A R 2016 Synthesis of monodispersed ag-doped bioactive glass nanoparticles via surface modification *Materials* **9** 225
- [44] Furtos G, Silaghi-dumitrescu L, Lewandowska K, Sionkowska A and Pascuta P 2015 Biocomposites for orthopedic and dental application *Key Eng. Mater.* **672** 261–75
- [45] Hench L L 1998 Bioceramics *J. Am. Ceram. Soc.* **81** 1705–28
- [46] Stoch A, Jastrzębski W, Brozek A, Trybalska B, Cichocińska M and Szarawara E 1999 FTIR monitoring of the growth of the carbonate containing apatite layers from simulated and natural body fluids *J. Mol. Struct.* **511–512** 287–94
- [47] Rámila A, Balas F and Vallet-Regí M 2002 Synthesis routes for bioactive sol-gel glasses: alkoxides versus nitrates *Chem. Mater.* **14** 542–8
- [48] El-Kady A, Rizk R and El-Hady B 2012 Characterization, and antibacterial properties of novel silver releasing nanocomposite scaffolds fabricated by the gas foaming/salt-leaching technique *J. Genet. Eng. Biotechnol.* **10** 229–38
- [49] Jones J R 2015 Review of bioactive glass: from Hench to hybrids *Acta Biomater.* **23** S53–82
- [50] Prabhu S and Poulouse E K 2012 Silver nanoparticles: mechanism of antimicrobial action, synthesis, medical applications, and toxicity effects *Int. Nano Lett.* **2** 32
- [51] Hu Q, Li Y, Miao G, Zhao N and Chen X 2014 Size control and biological properties of monodispersed mesoporous bioactive glass sub-micron spheres *RSC Adv.* **4** 22678
- [52] Tu J, Wang H, Li H, Dai K, Wang J and Zhang X 2009 The *in vivo* bone formation by mesenchymal stem cells in zein scaffolds *Biomaterials* **30** 4369–76
- [53] Wilding J P H, Woo V, Rohwedder K, Sugg J and Parikh S 2015 *In vitro* and *in vivo* evaluation of the developed PLGA/HAp/Zein scaffolds for bone-cartilage interface regeneration *Biomed. Environ. Sci.* **28** 1–12
- [54] Midha S, Kim T B, Van Den Bergh W, Lee P D, Jones J R and Mitchell C A 2013 Preconditioned 70S30C bioactive glass foams promote osteogenesis *in vivo* *Acta Biomater.* **9** 9169–82
- [55] Sepulveda P, Jones J R and Hench L L 2002 *In vitro* dissolution of melt-derived 45S5 and sol-gel derived 58S bioactive glasses *J. Biomed. Mater. Res.* **61** 301–11
- [56] Valerio P, Pereira M M, Goes A M and Leite M F 2004 The effect of ionic products from bioactive glass dissolution on osteoblast proliferation and collagen production *Biomaterials* **25** 2941–8
- [57] Xynos I D, Edgar A J, Buttery L D K K, Hench L L and Polak J M 2000 Ionic products of bioactive glass dissolution increase proliferation of human osteoblasts and induce insulin-like growth factor II mRNA expression and protein synthesis *Biochem. Biophys. Res. Commun.* **276** 461–5
- [58] Sabokbar A, Millett P J, Myer B and Rushton N 1994 A rapid, quantitative assay for measuring alkaline phosphatase activity in osteoblastic cells *in vitro* *Bone Miner.* **27** 57–67
- [59] Granéli C, Thorfve A, Ruetschi U, Brisby H, Thomsen P, Lindahl A and Karlsson C 2014 Novel markers of osteogenic and adipogenic differentiation of human bone marrow stromal cells identified using a quantitative proteomics approach *Stem Cell Res.* **12** 153–65
- [60] Golub E E and Boesze-Battaglia K 2007 The role of alkaline phosphatase in mineralization *Curr. Opin. Orthop.* **18** 444–8
- [61] Genge B R, Sauer G R, Wu L N Y, McLean F M and Wuthier R E 1988 Correlation between loss of alkaline phosphatase activity and accumulation of calcium during matrix vesicle-mediated mineralization *J. Biol. Chem.* **263** 18513–9
- [62] Sadat-Shojai M 2015 Calcium phosphate-reinforced polyester nanocomposites for bone regeneration applications *Biodegradable Polymeric Nanocomposites* ed D Depan (Boca Raton, FL: CRC Press) pp 1–34
- [63] Nuttelman C R, Kloxin A M and Anseth K S 2006 Temporal changes in peg hydrogel structure influence human mesenchymal stem cell proliferation and matrix mineralization *Adv. Exp. Med. Biol.* **585** 135–49
- [64] Stein G and Lian J 1993 Molecular mechanisms mediating developmental and hormone-regulated expression of genes in osteoblasts: an integrated relationship of cell growth and differentiation *Cellular Molecular Biology Bone* ed M Noda (Tokyo: Academic) pp 47–95
- [65] Liu X and Ma P X 2004 Polymeric scaffolds for bone tissue engineering *Ann. Biomed. Eng.* **32** 477–86
- [66] Zhang R Y and Ma P X 1999 Poly(alpha-hydroxyl acids) hydroxyapatite porous composites for bone-tissue engineering: I. Preparation and morphology *J. Biomed. Mater. Res.* **44** 446–55
- [67] Wang H-J, Gong S-J and Wang J-Y 2008 Mechanical improvement of zein protein as scaffold for bone tissue engineering *Mater. Sci. Technol.* **24** 1045–52
- [68] Barry J J A, Silva M M C G, Cartmell S H, Guldborg R E, Scotchford C A and Howdle S M 2006 Porous methacrylate tissue engineering scaffolds: using carbon dioxide to control porosity and interconnectivity *J. Mater. Sci.* **41** 4197–204
- [69] Mishra A, Rocherullé J and Massera J 2016 Ag-doped phosphate bioactive glasses: thermal, structural and *in vitro* dissolution properties *Biomed. Glass.* **2** 38–48